# Exotic correlation spread in free-fermionic states with initial patterns

Sudipto Singha Roy,<sup>1</sup> Giovanni Ramírez,<sup>2</sup> Silvia N. Santalla,<sup>3</sup> Germán Sierra,<sup>1</sup> and Javier Rodríguez-Laguna<sup>4</sup>

<sup>1</sup>Instituto de Física Teórica UAM/CSIC, Universidad Autónoma de Madrid, Cantoblanco, Madrid, Spain

<sup>2</sup>Instituto de Investigación, Escuela de Ciencias Físicas y Matemáticas,

Universidad de San Carlos de Guatemala, Guatemala

<sup>3</sup>Departamento de Física and Grupo Interdisciplinar de Sistemas Complejos (GISC), Universidad Carlos III de Madrid, Spain

<sup>4</sup>Departamento de Física Fundamental, UNED, Madrid, Spain

(Dated: January 25, 2022)

We describe a relation between the light-cone velocities after a quantum quench and the internal structure of the initial state, in the particular case of free fermions on a chain at half-filling. The considered states include short ranged valence bond solids, i.e. dimerized states, and long range states such as the rainbow. In all the considered cases the correlations spread into one or a few well-defined light-cones, each of them presenting an effective velocity which can be read from the form factor. Interestingly, we find that the observed velocities range from zero to the Fermi velocity and may not always be obtained from the dispersion relation for valid momenta.

#### I. INTRODUCTION

The spread of correlations is one of the central issues regarding the dynamics of quantum many-body systems. The main insight was provided by Lieb and Robinson<sup>1</sup>, when they proved rigorously that a light-cone structure appears within the dynamics of short-ranged Hamiltonians under some mild mathematical conditions on the nature of the interaction. Yet, it is relevant to ask about the effective velocity associated to the light-cone, and its relation to the propagation velocity of quasiparticles<sup>2</sup>, which is associated to the maximal group velocity according to the dispersion relations<sup>3,4</sup>, both in local and long-ranged Hamiltonians $^{5-7}$ , or in the case of periodically changing Hamiltonians<sup>8</sup>. The time evolution of the entanglement entropy (EE) under integrable Hamiltonians has received special attention. For example, non-equilibrium dynamics of EE after a sudden quantum quench has been extensively studied for the Ising model in a transverse field<sup>9</sup> or the XY model<sup>10</sup>. Recently, the exact time-evolution of the EE has been found for the XXZ model and the Lieb-Liniger model, showing a velocity dependence on the interaction parameters<sup>11,12</sup>. The non-integrable case presents its own challenges. For example, the Ising model subject to both a transversal and a longitudinal field shows that the spread of entanglement can be significatively faster than that of energy<sup>13</sup>. Moreover, the lightcone may fade away for some values of the interaction parameters, related to the interpretation of the Hamiltonian as a toy model for quark confinement 14, without violating the Lieb-Robinson result. It is shown that general hydrodynamical arguments yield a natural generalization of the group velocity<sup>15</sup>. An application of the conformal field theory (CFT) framework to quantum quench in the XX chain is also discussed $^{16}$ .

As the previous examples show, the effective velocity of the light-cone may vary with the interaction parameters and form. Yet, in some relatively recent works by Giovannini  $et\ al.^{17}$  and Bouchard  $et\ al.^{18}$  it is shown that spatially structured light-beams may propagate in vac-

uum with a speed lower than the speed of light, due to internal interference effects which give rise to an effective index of refraction. Thus, in some cases the lightcone velocity may depend significatively on the nature of the initial state. For example, it is known that thermal states present light-cone velocities correlated with the excess density of energy after a quench to the XXZ model<sup>19</sup>. Along with this, it has been shown that the presence of entanglement in the initial state can help in enhancing and accelerating the growth of correlations<sup>20</sup>. Moreover, we should stress the recent work by Najafi et al.<sup>21</sup>, where it is shown that initial states with a spatial periodicity can present a lower light-cone velocity under an XY Hamiltonian.

In this article, we extend the previous works by characterizing the spread of correlations in quantum states presenting different types of spatial structures under a spinless free-fermion Hamiltonian in one-dimension (1D), also known as the XX model, which is described in the continuum limit by a CFT. In many cases, correlations may spread into more than one light-cones. As we will show, the different light-cone velocities, which range from zero to the Fermi velocity, can be read from the form factor, i.e. the correlation matrix in momentum space. The behavior is also found to be imprinted in the growth of the EE where we report more than one linear stage of growth, with different slopes, corresponding to the passage of the different types of quasiparticles. We also extend the set of initial states, considering cases with short-range correlations, such as the dimerized state and a few more complex relatives, but also initial states with long-range correlations, such as the rainbow state and its variants<sup>22–31</sup>. By extending the formalism in the continuum limit, we show that in all the cases the structure of the correlation matrix away from the light-cone presents universal signatures: the correlations along the light-cone decay as  $t^{-1/3}$ .

This article is organized as follows. In section II we describe our model and initial states. Section III leads to our main result, showing how a spatial pattern in the initial correlation matrix may result in an effective ve-

locity different from the Fermi velocity. In section IV we discuss the implications of our results towards the time-evolution of the EE of different blocks. Section V discusses the universal features of the time-evolved correlation matrix away from the light-cone. We finish the paper in Sec. VI summarizing our conclusions and suggestions for further work.

# II. MODEL HAMILTONIAN AND INITIAL STATES

Our dynamics will be governed by the following free-fermionic Hamiltonian on a chain of size N,

$$H = -\frac{1}{2} \sum_{i=1}^{N} c_i^{\dagger} c_{i+1} + \text{h.c.},$$
 (1)

where  $c_i$  is the fermionic annihilation operators at site i, and where periodic boundaries are in effect,  $c_{N+1} = c_1$ . Let us define fermionic operators  $d_k$  with a well defined momentum

$$d_k = \frac{1}{\sqrt{N}} \sum_{j=1}^{N} e^{-ijk} c_j,$$
 (2)

where k ranges over the set of valid momenta,

$$k = \left\{ \frac{2m\pi}{N} \middle| m = 0, 1, 2, \dots, N - 1 \right\},$$
 (3)

transforming Hamiltonian (1) into

$$H = \sum_{k} \varepsilon_k \, d_k^{\dagger} d_k, \tag{4}$$

with eigenvalues  $\varepsilon_k = -\cos k$ .

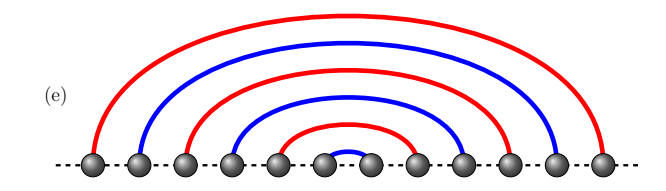
Let us choose a set of engineered states presenting spatial patterns, which we will allow to evolve under the action of Hamiltonian (1). Our first family of initial states are the  $Wigner\ crystals$  with period P, illustrated in Fig. 1 (a) and defined by

$$|W_P\rangle = \prod_{i=1}^{N/P} c_{Pi}^{\dagger} |0\rangle, \tag{5}$$

where N is divisible by P, and 1/P denotes the filling fraction. In this case, the group velocity for the excitations is given by

$$v_g = \frac{\partial \varepsilon_k}{\partial k} \bigg|_{k_F} = \sin\left(\frac{\pi}{P}\right).$$
 (6)





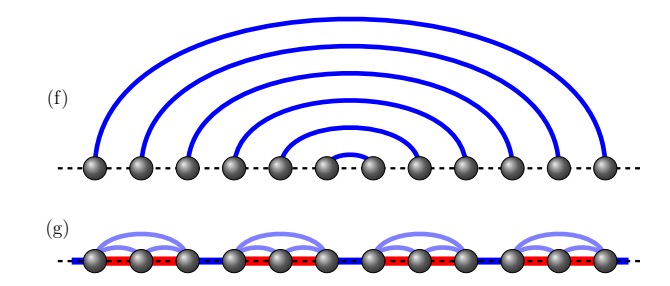


FIG. 1. Illustration of (a) Wigner state with P=3; (b) Dimer state; Dimer-q states, which present a spatial periodicity with P=4q sites, for (c) q=1 and (d) q=2; (e) Rainbow state, whose bonds alternate signs  $\eta_p$ , and (f) Frozen rainbow state, whose bonds always have the same sign  $\eta_p$ ; (g) Island-P states, which present spatial periodicity with P, for P=3.

This will be our only example away from half-filling. Most of our initial states will be *valence bond states* (VBS), defined by

$$|V\rangle \equiv 2^{-N/4} \prod_{p=1}^{N/2} (c_{l_p}^{\dagger} + \eta_p \, c_{r_p}^{\dagger}) |0\rangle,$$
 (7)

where the bond p connects sites  $l_p$  and  $r_p$ , with a relative phase  $\eta_p$ . We will assume that for all  $i \in \{1, \dots, N\}$  there is a unique p that satisfies either  $l_p = i$  or  $r_p = i$ , implying that all sites are part of a unique bond. Moreover, let us define the application  $\sigma : \{1, \dots, N\} \mapsto \{1, \dots, N\}$  such that  $\sigma_i$  yields the index of the partner of i, i.e.

$$\sigma_i = j \iff \exists p \mid (l_p = i \land r_p = j) \lor (l_p = j \land r_p = i).$$
 (8)

Our first VBS example is just the dimer state, Fig. 1 (b)

$$|D\rangle = 2^{-N/4} \prod_{p=1}^{N/2} \left( c_{2p-1}^{\dagger} + c_{2p}^{\dagger} \right) |0\rangle,$$
 (9)

i.e.  $l_p=2p-1, r_p=2p$  and  $\eta_p=1$  in Eq. (7). Of course,  $\sigma_i=i+1$  when i is odd, and i-1 when i is even. We will also consider some interesting generalizations, such as the dimer-q state, illustrated in Fig. 1 (c)-(d) and defined by

$$|D_q\rangle = 2^{-N/4} \prod_{p=1}^{N/2} \left( c_{2p-1}^{\dagger} + \Theta(p,q) c_{2p}^{\dagger} \right) |0\rangle,$$
 (10)

where  $\Theta(p,q)=(-1)^{\lfloor p/q\rfloor \mod 2}$ , i.e.: it alternates q bonds with  $\eta_p=+1$  sign and q bonds with  $\eta_p=-1$ . Therefore, the pattern repeats itself after exactly P=4q sites. Next, we consider the  $rainbow\ state^{22-30}$ , which is formed by a concentric set of bonds and presents maximal entropy between its left and right halves, as it is shown in Fig. 1 (e). It is defined as

$$|R\rangle = 2^{-N/4} \prod_{i=1}^{N/2} \left( c_i^{\dagger} + (-1)^{N/2+i} c_{N+1-i}^{\dagger} \right) |0\rangle.$$
 (11)

The rainbow state has received a great deal of attention because it can be built as the ground state (GS) of a deformed local Hamiltonian in the limit in which the inhomogeneity is large. We should stress that the form (11) describes the GS of some spin chains, such as the XX, XXZ or Ising chains<sup>25,28,31</sup>, after a Jordan-Wigner (JW) transformation has been applied, as it can be shown making use of the strong disorder renormalization group (SDRG) devised by Dasgupta and Ma<sup>32</sup>. The alternating character of the signs of its bonds can be understood in terms of the non-local nature of the JW transformation. Of course, it makes sense to define a rainbow state without sign alternation, which we will call the frozen rainbow for reasons to be understood later, see Fig. 1 (f).

Our last state will not be a VBS, yet it presents an interesting spatial periodic pattern, as shown in Fig. 1 (g). We will call it an *island-P* state,  $|I_P\rangle$ , and it is the GS of a Hamiltonian that can be written by weakening every P-th hopping amplitude from our original Hamiltonian (1),

$$H_P = H + \frac{\gamma}{2} \sum_{i=1}^{N/P} \left( c_{Pi}^{\dagger} c_{Pi+1} + \text{h.c.} \right),$$
 (12)

for  $\gamma \to 1^-$  (but  $\gamma \neq 1$  to avoid degeneracy), and N a multiple of P.

We would like to stress that most of these states are invariant under a spatial translation of P sites, but not the

rainbow states. Moreover, all of them can be described as Slater determinants, or Gaussian states, and as such they can be fully characterized by their correlation matrix, via Wick's theorem. In the case of a VBS defined by Eq. (7) we have

$$C_{j,j'} = \langle V | c_j^{\dagger} c_{j'} | V \rangle = \frac{1}{2} \left( \delta_{j,j'} + \eta_{p(j)} \delta_{j,\sigma(j')} \right). \tag{13}$$

Let us notice that all the considered states at half-filling (i.e. all of them except the Wigner states with P > 2) are GS of Hamiltonians with particle-hole symmetry, which implies that their density is exactly  $\langle c_i^{\dagger} c_i \rangle = 1/2$ .

# III. SPATIAL PATTERNS AND LIGHT-CONE VELOCITIES

In this section we provide the main result of this work, establishing a link between the spatial pattern of the initial state and the light-cone velocity or velocities needed to describe the time-evolved correlation matrix.

#### A. Free fermion dynamics

Let us describe the necessary set-up to analyze the time dynamics of the initial states introduced in the previous section under the free-fermionic Hamiltonian defined in Eq. (1). Let us consider an initial state  $|\psi\rangle$ , with correlation matrix  $C_{j,j'}$ . After a time t, we will have

$$|\psi(t)\rangle = e^{-itH}|\psi\rangle.$$
 (14)

Since all the considered states are Gaussian, we may characterize the time evolution from the two-point correlator,

$$C_{j,j'}(t) = \langle \psi(t) | c_j^{\dagger} c_{j'} | \psi(t) \rangle = \langle \psi(0) | c_j^{\dagger}(t) c_{j'}(t) | \psi(0) \rangle, \tag{15}$$

where  $c_j(t)$  is the fermion operator in the Heisenberg picture

$$c_{j}^{\dagger}(t) = e^{itH}c_{j}^{\dagger}e^{-itH} = \frac{1}{\sqrt{N}}\sum_{k}e^{-ijk}e^{it\varepsilon_{k}}d_{k}^{\dagger},$$
$$= \frac{1}{N}\sum_{k,\ell}e^{-i(j-\ell)k}e^{it\varepsilon_{k}}c_{\ell}^{\dagger}.$$
 (16)

Plugging this equation into Eq. (15) yields

$$C_{j,j'}(t) = \frac{1}{N^2} \Big[ \sum_{\substack{k,k'\\\ell,\ell'}} e^{-i(j-\ell)k+i(j'-\ell')k'} \ e^{it(\varepsilon_k - \varepsilon_{k'})} C_{\ell,\ell'} \Big].$$

(17)

Let us remind the reader that particle-hole symmetry implies that  $C_{j,j}(0) = 1/2$ , for all our initial states at half-filling. The density can be proved to remain constant for all time,  $C_{j,j}(t) = 1/2$ .

#### B. The Dimer State

The dimer case is specially simple and well-known, and deserves to be carried out in some detail. Applying Eq. (17) we obtain

$$C_{j,j'}(t) = \frac{\delta_{j,j'}}{2} + \frac{1}{4} \left( \delta_{j,j'-1} + \delta_{j,j'+1} \right) + \frac{(-1)^{j'}}{4N} \sum_{k} \left( e^{i(-j+j'-1)k} - e^{i(-j+j'+1)k} \right) e^{-2it\cos k},$$
(18)

which satisfies the initial condition

$$C_{j,j'}(t=0) = \frac{1}{2} \left( \delta_{j,j'} + \delta_{j,\sigma(j')} \right),$$
 (19)

in agreement with equation (13) for the dimer state. Observe that memory of the initial state is never really lost, because the long term time-average of the correlator yields the original value

$$\overline{C_{j,j'}} = \frac{1}{T} \int_0^T C_{j,j'}(t)dt \to \frac{\delta_{|j-j'|,1}}{4}.$$
 (20)

Notice also the time dependence  $e^{2it\varepsilon_k}$  in equation (18), which follows from the relation  $\varepsilon_{k+\pi} = -\varepsilon_k$ . In addition to this, the term  $(-1)^{j'}$  is responsible for a parity oscillation with respect to j'.

Let us consider the continuum limit of Eq. (18), approximating the sum by an an integral,

$$\frac{1}{N} \sum_{k} \to \frac{1}{2\pi} \int_{0}^{2\pi} dk,$$
 (21)

and defining x = j' - j. Then, for x > 1, we can replace Eq. (18) by

$$C(x,t) \simeq \frac{(-1)^{j'}}{8\pi} \int_0^{2\pi} \left[ e^{i(x-1)k} - e^{i(x+1)k} \right] e^{-2it\cos k} dk.$$
 (22)

Now, comparing the above integrals with the standard form of the Bessel function of first kind<sup>33</sup>,

$$J_n(\nu) = \frac{e^{i\frac{n\pi}{2}}}{2\pi} \int_0^{2\pi} e^{in\tau - i\nu\cos\tau} d\tau,$$
 (23)

we get

$$C(x,t) \simeq \frac{e^{i\frac{(j'+j+1)\pi}{2}}}{4} \left[ J_{x-1}(2t) + J_{x+1}(2t) \right].$$
 (24)

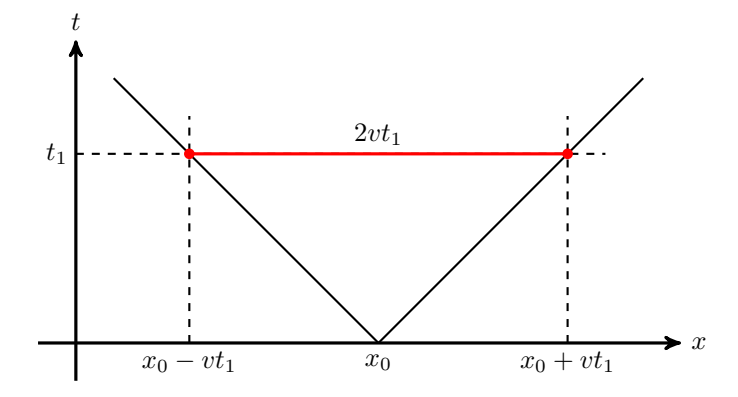


FIG. 2. Schematic representation of the propagation of a pair of quasiparticles with opposite velocities,  $\pm v$ , stemming from a point  $x_0$ . After a time  $t_1$ , the maximally correlated sites are located at a distance  $2vt_1=v_{\rm eff}t$ .

Notice that when the integrals are expressed in terms of Bessel functions, the phase between the two terms changes. At  $x \simeq 2t$  we can further approximate the above equation as follows,

$$C(x,t) \simeq \frac{e^{i\frac{(j'+j+1)\pi}{2}}}{2} J_x(2t).$$
 (25)

This expression shows that the correlation presents a light-cone structure, associated with an effective velocity  $v_{\rm eff}=2$ , since  $J_x(v_{\rm eff}t)\approx 0$  whenever  $x\gg v_{\rm eff}t$ . Notice that  $v_{\rm eff}$  is twice the Fermi velocity and apparently exceeds the Lieb-Robinson bound. The reason can be understood through the illustration of Fig. 2. Indeed, the initial state can be thought of as a source of quasiparticle excitations which emerge anywhere in the lattice  $(x_0)$  and propagate in opposite direction with the same velocity,  $\pm v$ . This results in a maximal correlation between sites located at a distance  $x=2vt=v_{\rm eff}t$  from each other.

The asymptotics of the Bessel function provides very valuable information about the structure of the correlation functions, both along and away from the light-cone, as we will consider in Sec. V.

## C. Form Factors

Let us define a form factor  $F_{k,k'}$  associated to the initial state  $|\psi(0)\rangle$  as

$$F_{k,k'} \equiv \langle \psi(0) | d_k^{\dagger} d_{k'} | \psi(0) \rangle = \frac{1}{N} \sum_{\ell,\ell'} e^{i(\ell k - \ell' k')} C_{\ell,\ell'},$$
(26)

which is just the Fourier transform of the initial correlation matrix, i.e. it corresponds to the correlation matrix in momentum space. Notice that  $|\langle \psi(t)|d_k^{\dagger}d_{k'}|\psi(t)\rangle|$  is preserved for all k and k' along the time evolution.

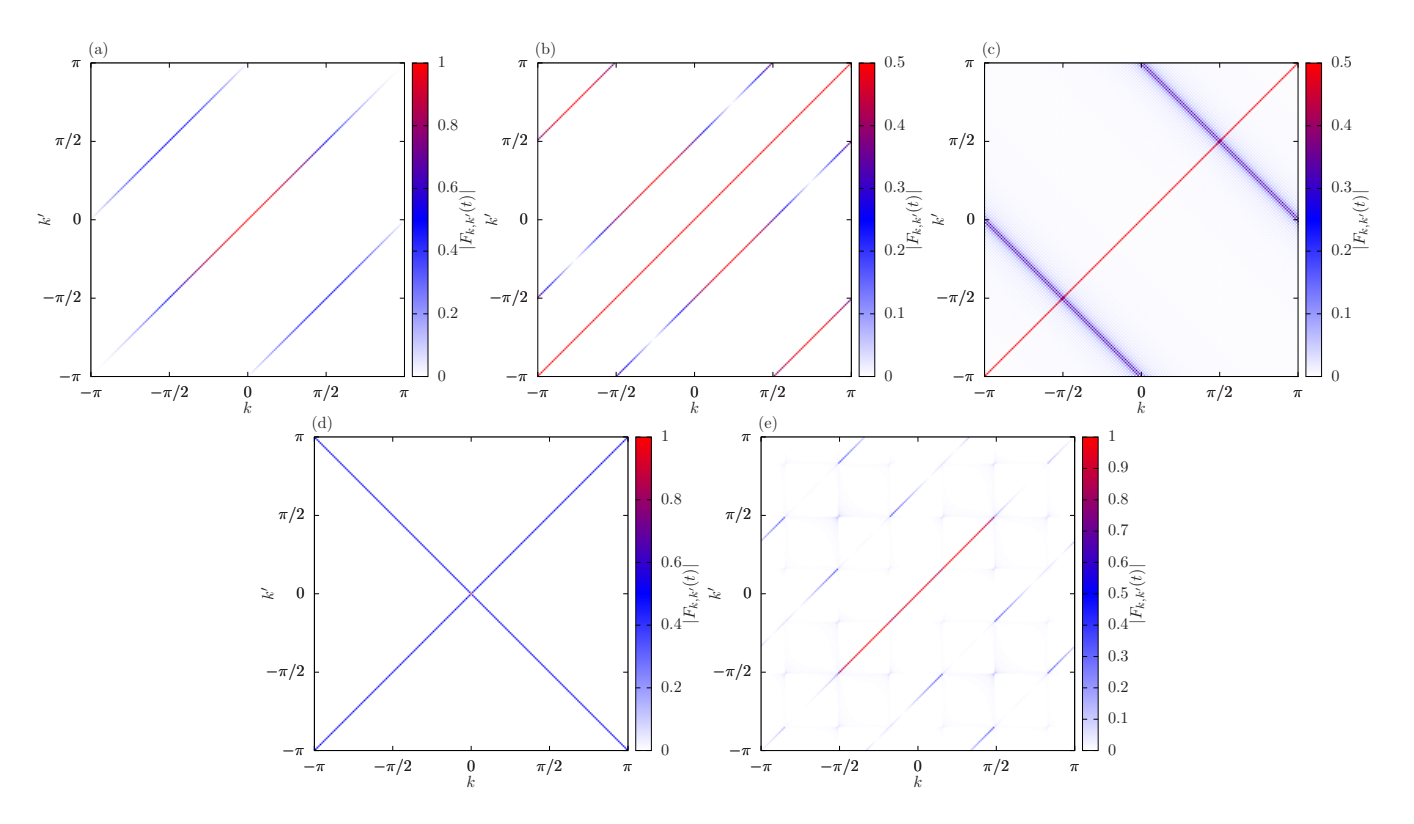


FIG. 3. Absolute value of the form factors  $|F_{k,k'}|$  for several relevant states, using N=240. The color code is chosen so as to provide a higher contrast. (a) Dimerized state, Eq. (9), (b) Dimer-1 state, Eq. (10), (c) Rainbow state, Eq. (11), (d) Frozen rainbow state, (e) Island-3 state, using  $\gamma = 1 - 10^{-2}$ .

Nonetheless, our definition Eq. (26) only makes reference to the initial state and does not have an absolute value. The form factor allows to simplify the expression for the time-evolved correlation matrix,

$$C_{j,j'}(t) = \frac{1}{N} \sum_{k,k'} e^{-i(jk-j'k')+it(\varepsilon_k - \varepsilon_{k'})} F_{k,k'}. \tag{27}$$

When the initial state is a VBS we can plug Eq. (13) into Eq. (26) to obtain

$$F_{k,k'} = \frac{1}{2} \delta_{k,k'} + \frac{1}{2N} \sum_{\ell=1}^{N} \eta_{p(\ell)} \left( e^{i(k\ell - k'\sigma(\ell))} \right).$$
 (28)

Let us evaluate the form factor of the states described in the previous section. For the dimer state, Eq. (9), we have

$$\begin{split} F_{k,k'} &= \frac{\delta_{k,k'}}{2} + \frac{1}{2N} \sum_{p=1}^{N/2} \left( e^{i((2p-1)k-2pk')} + e^{i(2pk-(2p-1)k')} \right) \\ &= \frac{\delta_{k,k'}}{2} + \frac{e^{ik'} + e^{-ik}}{2N} \sum_{p=1}^{N/2} e^{i2p(k-k')}, \\ &= \frac{\delta_{k,k'}}{2} + \frac{e^{ik'} + e^{-ik}}{4} \left( \delta_{|k-k'|=0} + \delta_{|k-k'|=\pi} \right), \quad (29) \end{split}$$

which is plotted in Fig. 3 (a), where we can observe two modulated straight lines: k' = k and  $k' = k \pm \pi$ . In a similar way, we can show that the form factor for the Wigner states of period P, Eq. (5) are given by

$$F_{k,k'} = e^{-i(k-k)} \frac{1}{2P} \sum_{m=0}^{P-1} \delta_{|k-k'|,2\pi m/P}.$$
 (30)

The exact calculation for the other relevant states is provided in the Appendix A, and here we will only report the results. For the dimer-q state we obtain

$$F_{k,k'} = \frac{\delta_{k,k'}}{2} + \frac{1}{4q} \left( \sum_{p=1}^{q} \left( \delta_{|k-k'|,\frac{\pi(2p-1)}{2q}} + \delta_{|k-k'|,2\pi - \frac{\pi(2p-1)}{2q}} \right) \right)$$

$$\left( \sum_{p=1}^{q} \left( e^{-i((2p-1)k-2(p-1)k')} + e^{-i(2(p-1)k-(2p-1)k')} \right) \right),$$
(31)

which means that it presents 2q parallel lines of the form  $k' = k \pm (2p-1)\pi/2q$ , as it is shown in Fig. 3 (b). On the other

$$F_{k,k'} = \frac{\delta_{k,k'}}{2} + \frac{(-1)^{N/2+1}e^{i\frac{k-k'}{2}}}{4N} \frac{\left(e^{i\frac{kN}{2}} + (-1)^{N/2+1}e^{-i\frac{k'N}{2}}\right)^2}{\cos(\frac{k+k'}{2})},$$
(32)

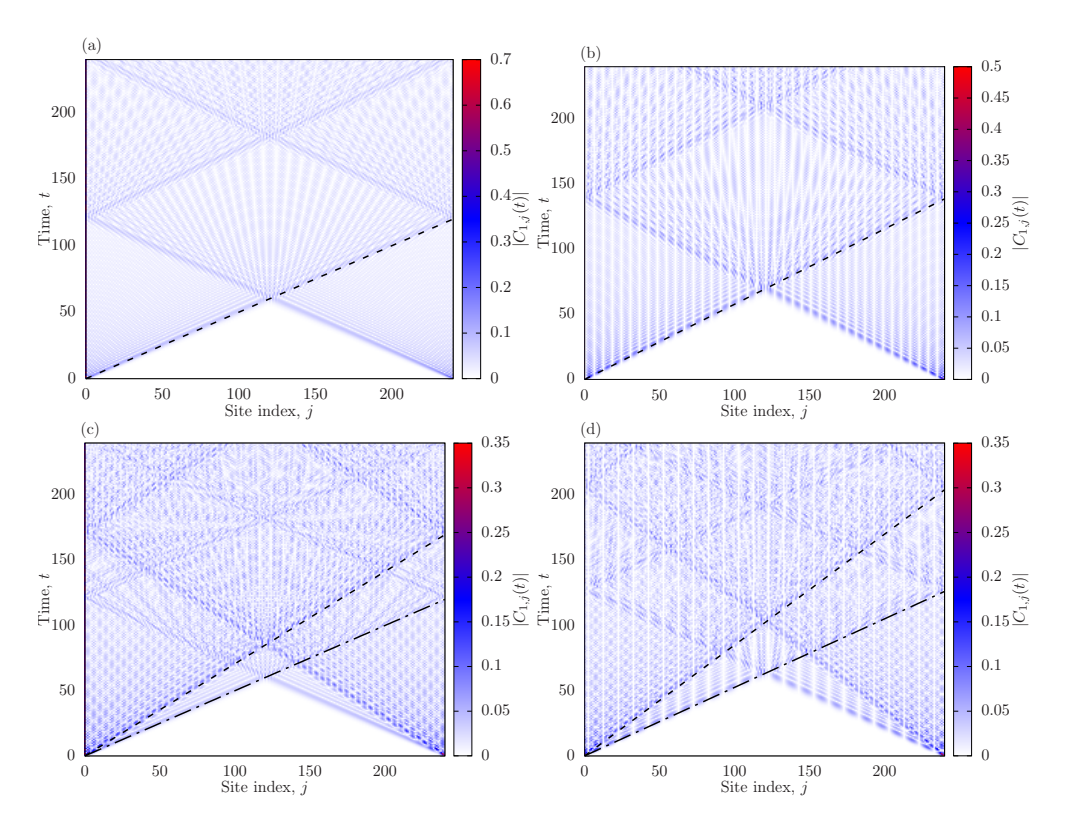


FIG. 4. Correlation maps  $|C_{1,j}(t)|$  for Wigner crystals, for different values of the periodicity with N = 240 for (a) P = 2, (b) P = 3, (c) P = 4 and (d) P = 5. The straight lines correspond to the theoretical predictions.

and it can be visualized in Fig. 3 (c). The denominator  $\cos((k+k')/2)$  shows that  $F_{k,k'}$  diverges whenever  $k+k'=\pm\pi$ , which yields the two orthogonal lines. The frozen rainbow has a simpler form factor,

$$F_{k,k'} = \frac{\delta_{k,k'}}{2} + \frac{e^{-i(N+1)k'}\delta_{|k+k'|=0}}{2},$$
 (33)

which yields the two orthogonal lines, k' = k and k' = -k, as we can see in Fig. 3 (d). Finally, we have numerically evaluated the form factor for the island-3 state, and check that it is approximately concentrated along straight lines of the form  $k' = k \pm 2\pi/3$  and  $k' = k \pm 4\pi/3$ .

#### D. Emergence of an effective velocity

In the previous section we realized that in many cases we can express the form factor in the following form

$$F_{k,k'} \approx \sum_{p} F_p(k)\delta(k \pm k' + \alpha_p),$$
 (34)

where  $F_p(k)$  is the modulation function and  $\alpha_p$  is the phase shift. Notice that this expression is exact in most cases, being approximate only for the rainbow and the island states. In this case, the time-evolved correlation matrix can be decomposed into a sum of terms, each

of which provides a light-cone with a different effective velocity, as we will prove.

The time-evolved correlation matrix, Eq. (27), can be written now as

$$C_{j,j'}(t) \equiv \sum_{p} \sum_{k} F_{p}(k) e^{-i(kj \mp (k+\alpha_{p})j')} e^{i(\varepsilon_{k} - \varepsilon_{\pm(k+\alpha_{p})})t},$$

$$= \sum_{p} C_{j,j'}^{(p)}(t)$$
(35)

and each p term can be evaluated as

$$C_{j,j'}^{(p)}(t) = e^{\pm i\alpha_p j'} \sum_{k} F_p(k) e^{-ik(j\mp j')} e^{-i(\cos(k) - \cos(k + \alpha_p))t},$$

$$= e^{\pm i\alpha_p j'} \sum_{k} F_p(k) e^{-ik(j\mp j')} e^{-i2\sin(k + \alpha_p/2)\sin(\alpha_p/2)t},$$

$$= e^{\pm i\alpha_p j'} \sum_{q} F_p(q) e^{i-((\pi - \alpha_p)/2 - q)(j\mp j')}$$

$$e^{-i\cos(q)(2\sin(\alpha_p/2)t)},$$
(36)

where in the last step we have defined  $q = (\pi - \alpha_p)/2 - k$ . Notice that the time dependence is completely encoded in the last term, and we can define an effective velocity

$$v_{\text{eff},p} = 2\sin(\alpha_p/2),\tag{37}$$

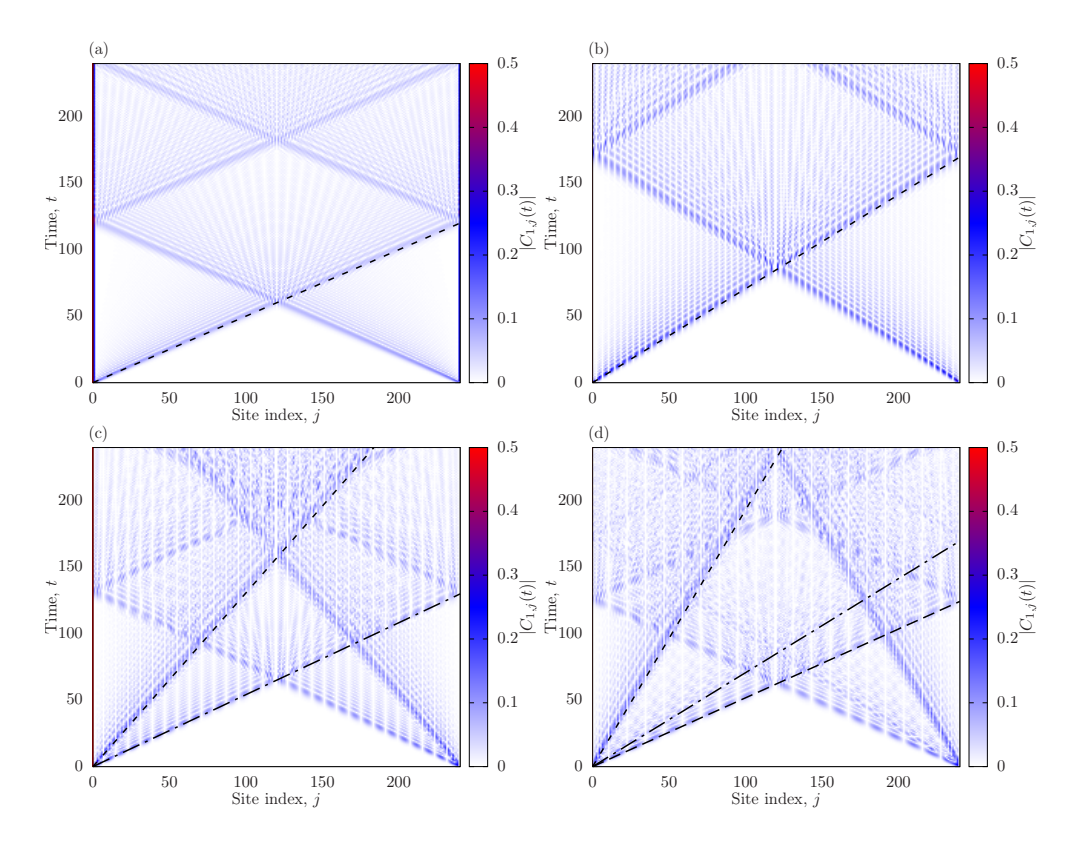


FIG. 5. Correlation maps  $|C_{1,j}(t)|$  for dimerized states, using N = 240. (a) Dimer state, (b) Dimer-1, (c) Dimer-2, and (d) Dimer-3. The straight lines correspond to the theoretical predictions.

thus allowing us to postulate that each straight line in the form factor diagram yields a term in the time-evolved correlation matrix, where the main difference is provided by the effective velocity. We are thus led to claim that our states may present different types of quasiparticles, characterized by different spreading velocities.

Moreover, we observe that once the velocity has been changed, the results are quite similar to those found for the dimer case, Eq. (25), thus allowing us to conjecture that the structure of the correlation functions will be similar in all the considered cases, once the time axis is scaled appropriately.

Let us check numerically the validity of expression (37), evaluating the time-evolution of the correlation matrix of the states discussed in Sec. II. In all the cases we will show the correlation  $|C_{1,j}(t)|$  using a colormap, with the second index in the horizontal axis and time in the vertical one.

Let us start with the Wigner crystals of period P, given in Eq. (5), even though they are not at half-filling for P > 2. The system size has been chosen in all the cases to be a multiple of P. Our theoretical prediction in this case is very clear, because the linear structure in the form factor is exact: the correlation matrix contains several terms, one corresponding to each line. The velocities are always given by

$$v_{\text{eff},m} = 2\sin\left(\frac{m}{P}\pi\right),$$
 (38)

with  $m \in \{1, \cdots, P-1\}$ . Thus, it will have a single light-cone for P=2 and P=3, which matches with the prediction given in P=3. However, we additionally show that for P>3 one gets more than one light-cone. Fig. 4 shows that this is indeed the case, using N=240. Notice that the innermost light-cone could have been predicted just by considering the group velocity at the corresponding filling factor, but our theoretical framework predicts all of them. Moreover, the outermost light-cone, is not predicted by the group velocity framework for P>3.

Next, let us check the validity of our results for the dimer state and its relatives, the dimer-q states. Our prediction for the dimer state is a single light-cone, with velocity  $v_{\rm eff}=2\sin(\pi/2)=2$ , which is indeed the case, as we can see in Fig. 5 (a). Yet, for alternating patterns of bonds and anti-bonds, we can observe lower velocities. For the dimer-1 state we have a single velocity,  $v_{\rm eff}=2\sin(\pi/4)=\sqrt{2}$ , which we can check in Fig. 5 (b). The situation for the dimer-2 and dimer-3 states is slightly more involved. In general, the velocities of the dimer-q states are given by

$$v_{\text{eff},p} = 2\sin\left(\frac{(2p-1)}{4q}\pi\right),\tag{39}$$

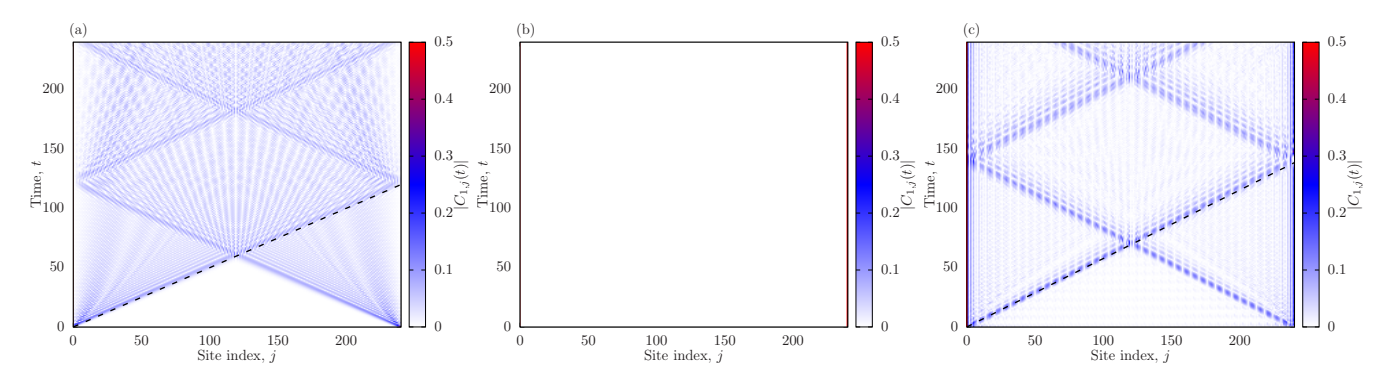


FIG. 6. Correlation maps  $|C_{1,j}(t)|$  for dimerized states, using N = 240. (a) Rainbow, (b) Frozen rainbow, (c) Island-3. The straight lines correspond to the theoretical predictions.

and we can see that for the dimer-2 the velocities are  $v_{\rm eff}=2\sin(\pi/8)$  and  $2\sin(3\pi/8)$ , as shown in Fig. 5 (c), while for the dimer-3, the velocities are  $v_{\rm eff}=2\sin(\pi/12)$ ,  $2\sin(3\pi/12)$  and  $2\sin(5\pi/12)$ , which are shown in Fig. 5 (d).

Next, let us consider the rainbow and the frozen-rainbow states. In Fig. 6 (a) we see the time-evolved correlation function  $|C_{1,j}(t)|$  for the rainbow state, which is very similar to that of the dimerized state. Indeed, our theoretical prediction is that there will be a single light-cone with velocity  $v_{\rm eff}=2\sin(\pi/2)=2$ . For the frozen rainbow our prediction is, on the other hand, that  $v_{\rm eff}=0$ , which is apparent from the absence of time-evolution in the correlation function that we can see in Fig. 6 (b). Indeed, the frozen rainbow can be proved to be an eigenstate of our Hamiltonian, Eq. (1).

Finally, let us consider the island-3 state, which is not a valence bond state, and is obtained as the ground state of Hamiltonian (12) with  $\gamma=1-10^{-3}$ . Indeed, the theoretical prediction based on the observation of the numerical form factor seen in Fig. 3 (e) is that we will obtain a single light-cone with  $v_{\rm eff}=2\sin(\pi/3)$ , which can be checked in the dashed straight line on the plot of Fig. 6 (c).

#### IV. ENTANGLEMENT GROWTH

The previous results have an impact on our predictions for the growth of the entanglement entropy of a block of size  $\ell$ . The quasiparticle picture devised by Cardy and Calabrese<sup>2</sup> provides the following Ansatz

$$S(\ell, t) = \begin{cases} \sigma v t, & \text{if } t < t_{\text{sat}}, \\ \sigma \ell, & \text{if } t > t_{\text{sat}}. \end{cases}$$
 (40)

where v is the effective velocity of the quasiparticles, and  $\sigma$  is the entropy per site of the stationary state after the quasiparticle wave has gone through the block. Of course, there may be more than one type of quasiparticles, and then the total entropy can be estimated as a

sum of terms of the form (40). Fig. 7 (a) shows the growth of EE for some of the states in our family, using always N=360 and  $\ell=50$ . Indeed, we can see that in some cases the single-quasiparticle picture is enough to predict the behavior, but for others we observe several regimes with different slopes, which correspond to the passage of different types of quasiparticles, with different velocities.

Fig. 7 (a) shows the EE of a left-most block of  $\ell=50$  sites out of a system with N=360 as a function of time, for several of our states. They all start in a linear way, as predicted by the quasiparticle picture, but they grow with different slopes. The saturation times for this first stage differ, since they are related to the fastest lightcone velocity present in the correlation function. In all cases, we have  $t_{\rm sat}=\ell/v_{\rm eff}$ , where  $v_{\rm eff}$  corresponds to the largest effective velocity. Moreover, the saturation values for the entropy are also very different among them, and we see that the dimer-q states reach the maximal possible value,  $S_{\rm sat}\approx \ell\log(2)$ , but the dimer and the island-3 do not.

The states with several light-cones, such as the dimer-2, dimer-3 and dimer-4, present more than one linear stage of growth, with different slopes, related to the passage of the different types of quasiparticles. Once the quickest ones have saturated, the slower ones still keep entangling the block with its environment, until they also saturate at a later time. At a time  $t=(L-\ell)/v_{\rm eff}$  the quickest particles have traveled around the whole system, and they start meeting again inside the initial block. We start a low entangling phase, in which the entanglement decreases linearly, reaching a lower value beyond which it starts growing again.

Let us consider the simplest case, that in which we obtain a single light-cone with a single speed. Among our examples, we have the dimer case, with  $v_{\rm eff}=2$ , the dimer-1 case, with  $v_{\rm eff}=2\sin(\pi/4)=\sqrt{2}$  and the island-3 case, with  $v_{\rm eff}=2\sin(\pi/3)=\sqrt{3}$ . Thus, we predict that the saturation times will be, respectively,  $t_{\rm sat}=\ell/v_{\rm eff}$  in all cases. Fig. 7 (b) shows the EE  $S/S_{\rm sat}$  divided by the saturation value, as a function of  $t/t_{\rm sat}$ , for a block  $\ell=50$  from a system with N=360 using

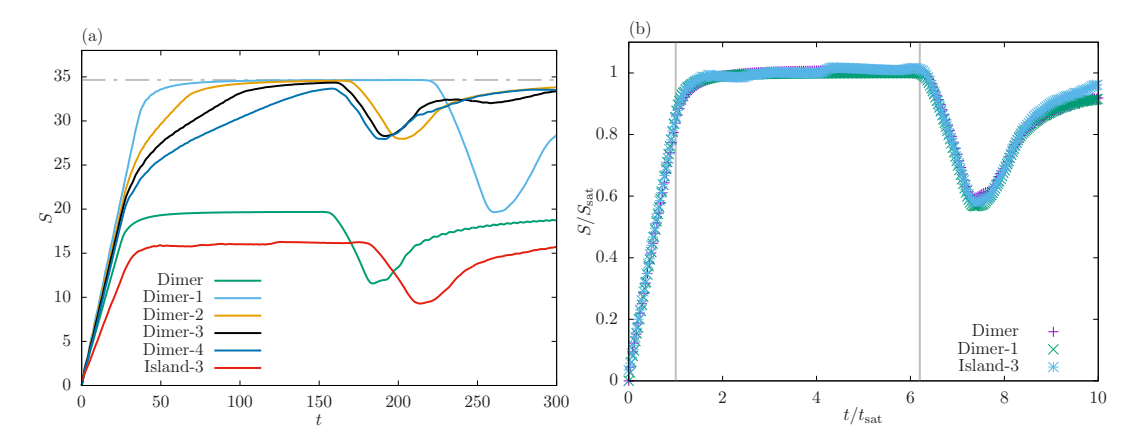


FIG. 7. (a) Time-evolution of the EE of certain selected states under the action of Hamiltonian (1) for N=360 and  $\ell=50$ . Notice that in some cases, such as the dimer, dimer-1 or island-3, the quasiparticle picture is fulfilled with a single velocity. Yet, for other states, such as dimer-2, dimer-3, we observe two different slopes, corresponding to the different types of quasiparticles. (b) When both the EE and time are rescaled by their saturation values, the data collapse for the three cases with a single light-cone, i.e. dimer, dimer-1 and island-3.

the dimer, dimer-1 and island-3 states. The data for the three systems collapse not only during the growth stage but also on the low entangling phase, both of which are marked by vertical lines.

#### V. UNIVERSAL FEATURES OF THE CORRELATION MATRIX

As we have checked both analytically and numerically, the time-evolution of the correlation function of the discussed states under the free-fermionic Hamiltonian presents one or several light-cones related to the patterns present in the initial state. In this section we will discuss the internal structure of this time-evolved correlation function, both on the light-cone and away from it. In the rest of this section we will consider that time has been rescaled such that

$$t \to v_{\text{eff}} t/2,$$
 (41)

and that we are considering a single contribution to the form factor, i.e. a single value of p in Eq. (34).

#### A. Asymptotic expansion along the light cone

Let us start with expression (25) for the time-evolved correlation function in the dimer case. The asymptotic expansions of  $J_x(2t)$  in the vicinity of the light cone x = 2t is given by

$$J_x(x) \sim \frac{2^{1/3}}{3^{2/3}\Gamma(2/3)} \frac{1}{x^{1/3}}, \quad x \to \infty.$$
 (42)

Now replacing  $J_{x-1}$  and  $J_{x+1}$  by  $J_x$ , we get

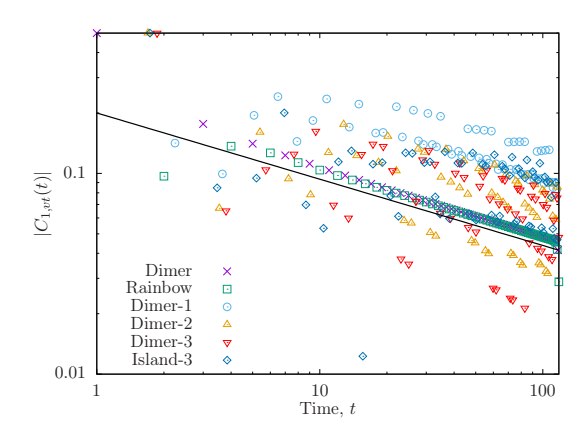


FIG. 8. Decay of the correlation between site 1 and site  $j=v_{\rm eff}t$  as a function of time for a system with N=240 sites, for most of our initial states, using always the maximal velocity  $v_{\rm eff}$  for which a light-cone appears. The continuous black straight line correspond to the theoretical prediction,  $C\sim t_{-1/3}$ 

$$C(x=2t) \approx \frac{e^{i\frac{(j'+j+1)\pi}{2}}}{23^{2/3}\Gamma(2/3)} \frac{1}{t^{1/3}}.$$
 (43)

This implies a behavior  $t^{-1/3}$  for the correlator exactly on the light cone x=2t. This behavior is expected in all our cases, since the correlation matrix is a sum of terms, each one of them associated to a light-cone, and all of them presenting a behavior similar to (43). Indeed, this is proved to be the case in Fig. 8, where we show the decay along the light-cone of the correlation for most of our states, always using N=240. For the dimer and the rainbow the power-law decay is very clean. For all the other states we have chosen the most intense light-cone, and the results present oscillations which partially mask the universal features. Yet, we can see that in

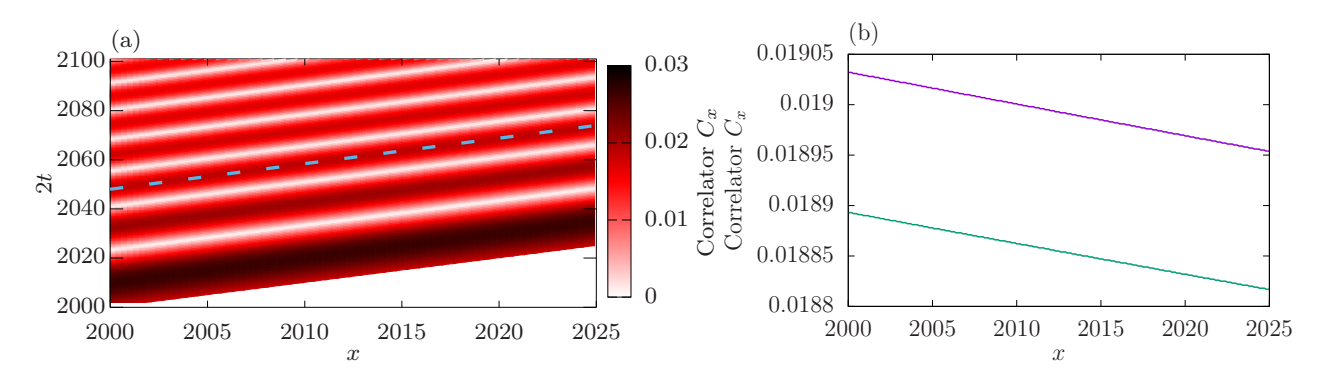


FIG. 9. (a) Space-time diagram of the evolution of the correlation of the dimer state after a quench obtained using Eq. (25) for the region  $x \gg 1$ . The diagram shows the correlation between the left-most site with all other sites,  $C_x = |\langle \Psi(t)|c_1^{\dagger}c_{1+x}|\Psi(t)\rangle|$ . Each of the lines approximately corresponds to a maxima (or a minima) of  $|C_x|$  that can be obtained by putting the argument of cosine in Eq. (49) to be integer (half integer) multiple of  $\pi$ . For instance, the dashed line corresponds to a maxima of  $|C_x|$  where the argument of cosine in Eq. (49) takes the value  $2\pi$ . (b) Comparison of the values of correlator  $|C_x|$  obtained using Eqs. (25) (violet) and (49) (green) along the dashed line shown in Fig. 9.

all the considered cases (dimer-1, dimer-2, dimer-3 and island states) the  $t^{-1/3}$  scaling is respected to a good approximation.

## B. Asymptotic expansion away from light cone

There is another interesting asymptotic behavior that emerges following the approximation of the Bessel functions<sup>33</sup>, given by

$$J_{\nu}(\nu + z\nu^{1/3}) \sim (2/\nu)^{1/3} \operatorname{Ai}(-2^{1/3}z), \quad \nu \to \infty \quad (44)$$

where Ai(z') is the Airy function. Now one can use the asymptotic behavior of Ai(z') given by

$$\operatorname{Ai}(-z') \sim \pi^{-1/2} z'^{-1/4} \sin(\zeta + \pi/4), |z'| \gg 1,$$
(45)

and consider z' > 0, with  $\zeta = \frac{2}{3}z'^{3/2}$ . Plugging (45) into (44) yields

$$J_{\nu}(\nu + z\nu^{1/3}) \sim \frac{2^{1/4}}{\pi^{1/2}\nu^{1/3}z^{1/4}} \cos\left(\frac{(2z)^{3/2}}{3} - \frac{\pi}{4}\right).$$
 (46)

These expressions give the asymptotics of  $J_x(2t)$  with the identifications

$$x = \nu$$
,  $2t = \nu + z\nu^{1/3} \to z = \frac{2t - x}{r^{1/3}}$ . (47)

Plugging that into Eq. (46) we get

$$J_x(x+zx^{1/3}) \sim \frac{2^{1/4}}{\pi^{1/2}x^{1/4}(2t-x)^{1/4}}$$
$$\cos\left(\frac{(4t-2x)^{3/2}}{3x^{1/2}} - \frac{\pi}{4}\right), \quad (48)$$

which may lead to another prediction for the correlators within the light cone,

$$C(x,t) \simeq \frac{e^{i\frac{(j'+j+1)\pi}{2}}}{2^{3/4}\pi^{1/2}x^{1/4}(2t-x)^{1/4}}\cos\left(\frac{(4t-2x)^{3/2}}{3x^{1/2}} - \frac{\pi}{4}\right)$$
(49)

In Fig. 9 (a) we plot the behavior of C(x,t) obtained using Eq. (25), for the region  $x\gg 1$  and identify that the maximum (minimum) in Fig. 9 (a) are obtained when the argument of cosine in Eq. (49) becomes integer (half integer) multiple of  $\pi$ . For instance, the dashed line in Fig. 9 (a) corresponds to  $\frac{(4t-2x)^{3/2}}{3x^{1/2}} - \frac{\pi}{4} = 2\pi$ . Hence, one can find that along such lines, correlators again approximately behave similar to the light-cone,

$$C(x,t) \simeq \frac{e^{i\frac{(j'+j+1)\pi}{2}}}{2^{3/4}\pi^{1/2}x^{1/3}z^{1/4}}.$$
 (50)

An exact comparison of  $|C_x|$  obtained using Eq. (25) to that obtained using Eq. (49) along this line is presented in Fig. 9 (b).

## VI. CONCLUSIONS AND FURTHER WORK

We have considered the time-evolution of several quantum states on a periodic chain with spatial patterns under the massless free fermion Hamiltonian, finding that all of them present one or several light-cones with different velocities, which can be read from the form factor, i.e. the initial correlation matrix in momentm space. As we have been able to check, in all the considered cases the form factor is concentrated on straight lines, and the momentum shift associated to each of them provides an effective light-cone velocity. In some cases we were able to find a single light-cone, but with a velocity lower than

the Fermi velocity associated to the considered Hamiltonian and filling factor, bearing some similarities to the recent experiments in which a light beam can be seen to propagate in vacuum with a velocity lower than c, due to interference effects associated to its internal structure.

Moreover, we have found that this complex light-cone structure shows up in the time-evolution of the entanglement entropy. In the case of initial states which give rise to a single light-cone we were able to collapse the EE as we rescale both time and the entropy to its maximal saturation value, which also differs from one state to others. Yet, for the complex light-cone structures we observe that the EE growth presents several linear regimes before saturation. This behavior can be explained within the quasiparticle picture, if we assume that there are several species of quasiparticles. We would like to remark that the entropy production depends on the initial state. In our case, the dimer-q states reach the maximum possible value for the entropy,  $S_{\text{sat}} = \ell \log(2)$ , while other states seem to reach lower values for the saturation, implying that their quasiparticles do not carry enough entanglement among them.

It is relevant to ask about the nature of these quasiparticles, which is hidden inside the form factor. Indeed, it can be shown that certain pairs of momenta are strongly entangled among themselves, and this entanglement is preserved along the time-evolution. For example, the frozen rainbow state entangles momenta k and -k, and

the dimer state entangles momenta k and  $k \pm \pi$ . An analysis of entanglement in Fourier space would be of much help to elucidate this question<sup>34</sup>.

Beyond the existence of the light-cone and its velocity, we found that each straight line term in the form factor gives rise to a term in the correlation matrix that decays like  $t^{-1/3}$  at large distances. Moreover, the lost correlation spreads away from the light-cone in a way that is also predicted by the theory in the continuum limit.

It is relevant to ask whether these structures can be seen in interacting systems, either integrable or nonintegrable. The dynamics of interacting systems is very different from the free theory considered in our case, because our form factor is preserved through the evolution.

#### ACKNOWLEDGMENTS

We thank Pasquale Calabrese, Erik Tonni, Vincenzo Alba for conversations. We also thank Jacopo Viti for his useful comments on our work. We acknowledge the Spanish government for financial support through grants PGC2018-095862-B-C21, PGC2018-094763-B-I00, PID2019-105182GB-I00, Comunidad de Madrid grant No. S2018/TCS-4342, SEV-2016-0597 of the "Centro de Excelencia Severo Ochoa" Programme and the CSIC Research Platform on Quantum Technologies PTI-001.

#### Appendix A: Computation of the form factors

In this appendix we evaluate the exact form factors for some of the states discussed in the main text.

## 1. Form factor for the rainbow state

Let us now compute the form factor for the rainbow state as follows.

$$F_{k,k'} = \frac{1}{2N} \sum_{\ell} \left( \left[ (-1)^{\eta_{\ell}} e^{i(\ell k - \sigma(\ell)k')} + e^{i(k\sigma(\ell) - \ell k')} \right] + \left[ e^{i(\ell k - \ell k')} + e^{i(\sigma(\ell)k - \sigma(\ell)k')} \right] \right),$$

$$= \frac{1}{2N} \sum_{\ell=1}^{N/2} (-1)^{\ell + N/2} \left[ e^{i(k\ell - (N+1-\ell)k')} + e^{i(k(N+1-\ell)-\ell k')} \right] + \frac{1}{2N} \sum_{\ell=1}^{N/2} \left[ e^{i\ell(k-k')} + e^{i(N+1-\ell)(k-k')} \right], \quad (A1)$$

where we have used  $\ell \in \mathcal{A} = \{1, 2, 3, \dots N/2\}$ , and  $\sigma(\ell) \in \bar{\mathcal{A}} = N, N-1, \dots N+1-\ell$ ,  $\eta_{\ell} = N/2+\ell$ . Now let us consider each term separately.

$$\frac{1}{2N} \sum_{\ell=1}^{N/2} (-1)^{\ell+N/2} \left[ e^{i(k\ell-(N+1-\ell)k')} \right],$$

$$= \frac{1}{2N} e^{-ik'(N+1)} \sum_{\ell=1}^{N/2} (-1)^{\ell+N/2} e^{i\ell(k+k')}.$$
(A2)

Now using the formula  $\sum_{n=0}^{N/2} x^n = \frac{x^{N/2+1}-1}{x-1}$ , and thus  $\sum_{n=1}^{N/2} x^n = \frac{x^{N/2+1}-1}{x-1} - 1 = \frac{x^{N/2+1}-x}{x-1}$ , we get

$$\frac{(-1)^{N/2}}{2N}e^{-ik'(N+1)} \sum_{\ell=1}^{N/2} (-1)^{\ell} e^{i\ell(k+k')},$$

$$= \frac{(-1)^{N/2+1}}{2N} e^{-ik'(N+1)} \left[ \frac{(-1)^{N/2+1} e^{i(N/2+1)(k+k')} + e^{i(k+k')}}{e^{i(k+k')} + 1} \right].$$
(A3)

Similarly, for the second term, in Eq. (A3) we have to replace k by -k' and we will get

$$\frac{(-1)^{N/2}}{2N}e^{ik(N+1)} \sum_{\ell=1}^{N/2} (-1)^{\ell} \left[ e^{-i\ell(k+k')} \right],$$

$$= \frac{(-1)^{N/2+1}}{2N}e^{ik(N+1)} \left[ \frac{(-1)^{N/2+1}e^{-i(N/2+1)(k+k')} + e^{-i(k+k')}}{e^{-i(k+k')} + 1} \right],$$
(A4)

Whereas the third and the fourth term give

$$\frac{1}{2N} \sum_{\ell=1}^{N/2} \left[ e^{i\ell(k-k')} + e^{i(N+1-\ell)(k-k')} \right],$$

$$= \frac{\delta_{k,k'}}{2}.$$
(A5)

Now plugging these back in Eq. (A1), we get

$$F_{k,k'} = \frac{(-1)^{N/2}}{2N} \sum_{\ell=1}^{N/2} (-1)^{\ell} \left[ e^{i(k\ell - (N+1-\ell)k')} + e^{i(k(N+1-\ell)-\ell k')} \right] + \frac{1}{2N} \sum_{\ell=1}^{N/2} \left[ e^{i\ell(k-k')} + e^{i(N+1-\ell)(k-k')} \right],$$

$$= \frac{(-1)^{N/2+1}}{4N} \frac{e^{i\frac{k-k'}{2}} \left( e^{ikN/2} + (-1)^{N/2+1} e^{-ik'N/2} \right)^2}{\cos(\frac{k+k'}{2})} + \frac{\delta_{k,k'}}{2}.$$
(A6)

## 2. Form factor for frozen-rainbow

The form factor for the frozen-rainbow state for  $|k+k'| \neq 0, 2\pi, 4\pi$  is given by

$$F_{k,k'} = \frac{1}{2N} \sum_{\ell=1}^{N/2} \left[ e^{i(k\ell - (N+1-\ell)k')} + e^{i(k(N+1-\ell)-\ell k')} \right] + \frac{1}{2N} \sum_{\ell=1}^{N/2} \left[ e^{i\ell(k-k')} + e^{i(N+1-\ell)(k-k')} \right],$$

$$= \frac{1}{2N} \left[ e^{-ik'(N+1)} \frac{e^{i(k+k')(N/2+1)} - e^{i(k+k')}}{e^{i(k+k')} - 1} + e^{ik(N+1)} \frac{e^{-i(k+k')(N/2+1)} - e^{-i(k+k')}}{e^{-i(k+k')} - 1} \right]$$

$$= \frac{1}{2N} \left[ \frac{e^{ik(N/2+1)-ik'N/2} - e^{ik-ik'N}}{e^{i(k+k')} - 1} + \frac{e^{ikN/2-ik'(N/2+1)} - e^{ikN-ik'}}{e^{-i(k+k')} - 1} \right] + \frac{\delta_{k,k'}}{2}. \tag{A7}$$

Whereas, for  $|k + k'| = 0, 2\pi, 4\pi F_{k,k'}$  is given by

$$F_{k,k'} = \frac{e^{-ik'(N+1)} + e^{ik(N+1)}}{4} + \frac{\delta_{k,k'}}{2},$$

$$= \frac{e^{-ik'(N+1)}}{2} \delta_{|k+k'|,0} + \frac{\delta_{k,k'}}{2}.$$
(A8)

#### 3. Form factor for the Dimer-1

We derive the form factor for dimer-1 state as follows.

$$F_{k,k'} = \frac{1}{2N} \sum_{\ell=1}^{N/2} \left( \left[ (-1)^{\eta_{\ell}} e^{i(\ell k - \sigma(\ell)k')} + e^{i(k\sigma(\ell) - \ell k')} \right] + \left[ e^{i(\ell k - \ell k')} + e^{i(\sigma(\ell)k - \sigma(\ell)k')} \right] \right),$$

$$= \frac{1}{2N} \sum_{\ell=1}^{N/2} \left( \left[ (-1)^{\ell} e^{i[(2\ell - 1)k - 2\ell k']} + e^{i[k2\ell - (2\ell - 1)k']} \right] + \left[ e^{i(\ell k - \ell k')} + e^{i(\sigma(\ell)k - \sigma(\ell)k')} \right] \right),$$

$$= \frac{1}{2N} \left( e^{-ik} \sum_{\ell=1}^{N/2} (-1)^{\ell} e^{i2\ell(k - k')} + e^{ik'} \sum_{\ell=1}^{N/2} (-1)^{\ell} e^{i(\ell k - \ell k')} \right) + \frac{\delta_{|k - k'|, 0}}{2},$$

$$F_{k,k'} = \frac{e^{-ik} + e^{ik'}}{4} \left( \delta_{|k - k'|, \pi/2} + \delta_{|k - k'|, 3\pi/2} \right) + \frac{\delta_{|k - k'|, 0}}{2}.$$
(A9)

## 4. Form factor for the Dimer-2 and any general Dimer-q state

We now aim to derive the form factor of dimer-q state for any general q. For that we first present the case for q=2.

$$\begin{split} F_{k,k'} &= \frac{1}{2N} \Big( \sum_{\ell=1}^{N/4} (-1)^{\eta_{\ell}} \Big[ e^{i(k(4\ell-3)-k'(4\ell-2))} + e^{i(k(4\ell-1)-k'(4\ell))} \Big] + \sum_{\ell=1}^{N/4} (-1)^{\eta_{\ell}} \Big[ e^{i(k(4\ell-2)-k'(4\ell-3))} + e^{i(k(4\ell)-k'(4\ell-1))} \Big] \Big) \\ &+ \sum_{\ell=1}^{N/2} \Big[ e^{i(\ell k-\ell k')} + e^{i(\sigma(\ell)k-\sigma(\ell)k')} \Big] \Big), \end{split} \tag{A10} \\ &= \frac{1}{2N} \Big( e^{-i(3k-2k')} \sum_{\ell=1}^{N/4} (-1)^{\eta_{\ell}} e^{i(4\ell(k-k'))} + e^{-ik} \sum_{\ell=1}^{N/4} (-1)^{\eta_{\ell}} e^{i(4\ell(k-k'))} + e^{i(3k'-2k)} \sum_{\ell=1}^{N/4} (-1)^{\eta_{\ell}} e^{i(4\ell(k-k'))} \\ &+ e^{ik'} \sum_{\ell=1}^{N/4} (-1)^{\eta_{\ell}} e^{i(4\ell(k-k'))} \Big) + \frac{\delta_{k,k'}}{2}, \\ &= \frac{1}{8} \Big( e^{-i(3k-2k')} (\delta_{[k-k'],\frac{\pi}{4}} + \delta_{[k-k'],\frac{3\pi}{4}} + \delta_{[k-k'],\frac{5\pi}{4}} + \delta_{[k-k'],\frac{\pi}{4}} \Big) + e^{-ik} \Big( \delta_{[k-k'],\frac{\pi}{4}} + \delta_{[k-k'],\frac{3\pi}{4}} + \delta_{[k-k'],\frac{7\pi}{4}} \Big) + e^{i(3k'-2k)} \Big( \delta_{[k-k'],\frac{\pi}{4}} + \delta_{[k-k'],\frac{3\pi}{4}} + \delta_{[k-k'],\frac{7\pi}{4}} \Big) \Big), \\ &+ \frac{\delta_{k,k'}}{2}, \end{aligned} \tag{A11} \\ &= \frac{1}{8} \Big( \delta_{[k-k'],\frac{\pi}{4}} + \delta_{[k-k'],\frac{3\pi}{4}} + \delta_{[k-k'],\frac{5\pi}{4}} + \delta_{[k-k'],\frac{7\pi}{4}} \Big) \Big( e^{-i(3k-2k')} + e^{-ik} + e^{i(3k'-2k)} + e^{ik'} \Big) + \frac{\delta_{k,k'}}{2}. \end{aligned} \tag{A12}$$

Hence, the form factor for any general dimer-q state is given by

$$F_{k,k'} = \frac{\delta_{k,k'}}{2} + \frac{1}{4q} \left( \sum_{p=1}^q \left( e^{-i((2p-1)k-2(p-1)k')} + e^{-i(2(p-1)k-(2p-1)k')} \right) \right) \left( \sum_{p=1}^q \left( \delta_{|k-k'|,\frac{\pi(2p-1)}{2q}} + \delta_{|k-k'|,2\pi-\frac{\pi(2p-1)}{2q}} \right) \right). \tag{A13}$$

<sup>&</sup>lt;sup>1</sup> E. H. Lie and D. W. Robinson, *The finite group velocity of quantum spin systems*, Comm. Math. Phys. **28**, 251 (1972).

<sup>&</sup>lt;sup>2</sup> P. Calabrese and J. Cardy, Evolution of entanglement entropy in one-dimensional systems, J. Stat. Mech. P04010 (2005).

<sup>&</sup>lt;sup>3</sup> G. De Chiara, S. Montangero, P. Calabrese, and R. Fazio, Entanglement entropy dynamics of Heisenberg chains, J. Stat. Mech. P03001 (2006).

<sup>&</sup>lt;sup>4</sup> M. Fagotti and P. Calabrese, Evolution of entanglement entropy following a quantum quench: Analytic results for

the XY chain in a transverse magnetic field, Phys. Rev. A **78**, 010306(R) (2008).

<sup>5</sup> A. M. Läuchli and C. Kollath, Spreading of correlations and entanglement after a quench in the one-dimensional Bose-Hubbard model, J. Stat. Mech. P05018 (2008).

<sup>6</sup> M. G. Nezhadhaghighi and M. A. Rajabpour, Entanglement dynamics in short-and long-range harmonic oscillators, Phys. Rev. B 90, 205438 (2014).

- A. S. Buyskikh, M. Fagotti, J. Schachenmayer, F. Essler, and A.J. Daley, Entanglement growth and correlation spreading with variable-range interactions in spin and fermionic tunneling models, Phys. Rev. A 93, 053620 (2016).
- <sup>8</sup> V. Eisler and I. Peschel, Entanglement in a periodic quench, Ann. Phys. (Berlin) 17, 410 (2008).
- L. Bucciantini. M. Kormos, and P. Calabrese, Quantum quenches from excited states in the Ising chain, J. Phys. A: Math. Theor. /bf 47, 175002 (2014).
- M. Fagotti and M. Collura, Universal prethermalization of entanglement entropies after a global quench, arXiv:1507.02678 [quant-ph](2015).
- V. Alba and P. Calabrese, Entanglement and thermodynamics after a quantum quench in integrable systems, Proc. Nat. Acad. Sci. 114, 7947 (2017).
- <sup>12</sup> V. Alba and P. Calabrese, Entanglement dynamics after quantum quenches in generic integrable systems, SciPost Phys. 4, 017 (2018).
- <sup>13</sup> H. Kim and D. A. Huse, Ballistic spreading of entanglement in a diffusive nonintegrable system, Phys. Rev. Lett. 111, 127205 (2013).
- <sup>14</sup> M. Kormos, M. Collura, G. Takács, and P. Calabrese, Real-time confinement following a quantum quench to a non-integrable model, Nature Phys. 13, 246 (2017).
- <sup>15</sup> G. Perfetto and B. Doyon, Euler-scale dynamical fluctuations in non-equilibrium interacting integrable systems, Sci-Post Phys. 10, 116 (2021).
- <sup>16</sup> N. Allegra, J. Dubail, J. M. Stéphan and J. Viti, *Inhomogeneous field theory inside the arctic circle*, J. Stat. Mech. **053108** (2016).
- <sup>17</sup> D. Giovannini et al., Spatially structured photons that travel in free space slower than the speed of light, Science 347, 857 (2015).
- <sup>18</sup> F. Bouchard et al., Observation of subluminal twisted light in vacuum, Optica 3, 351 (2016).
- <sup>19</sup> L. Bonnes, F. H. L. Essler, and A. M. Läuchli, "Light-cone" dynamics after quantum quenches in spin chains, Phys. Rev. Lett. 113, 187203 (2014).

- <sup>20</sup> M. Kastner, Entanglement-enhanced spreading of correlations, New J. Phys. 17, 123024 (2015)
- <sup>21</sup> K. Najafi, M. A. Rajabpour, and J. Viti, Light-cone velocities after a global quench in a noninteracting model, Phys. Rev. B 97, 205103 (2018).
- <sup>22</sup> G. Vitagliano, A. Riera, and J.I. Latorre, Volume-law scaling for the entanglement entropy in spin 1/2 chains, New J. Phys. 12, 113049 (2010).
- <sup>23</sup> G. Ramírez, J. Rodríguez-Laguna, and G. Sierra, From conformal to volume-law for the entanglement entropy in exponentially deformed critical spin 1/2 chains, J. Stat. Mech. P10004 (2014).
- <sup>24</sup> G. Ramírez, J. Rodríguez-Laguna, and G. Sierra, Entanglement over the rainbow, J. Stat. Mech. P06002 (2015).
- J. Rodríguez-Laguna, S.N. Santalla, G. Ramírez, and G. Sierra, Entanglement in correlated random spin chains, RNA folding and kinetic roughening, New J. Phys. 18, 073025 (2016).
- J.Rodríguez-Laguna, J. Dubail, G. Ramírez, P. Calabrese, and G. Sierra, More on the rainbow chain: entanglement, space-time geometry and thermal states, J. Phys. A: Math. Theor. 50, 164001 (2017).
- <sup>27</sup> E. Tonni, J. Rodríguez-Laguna, and G. Sierra, Entanglement hamiltonian and entanglement contour in inhomogeneous 1D critical systems, J. Stat. Mech. 043105 (2018).
- N. Samos Sáenz de Buruaga, S.N. Santalla, J. Rodríguez-Laguna, and G. Sierra Symmetry protected phases in inhomogeneous spin chains, J. Stat. Mech. 093102 (2019).
- <sup>29</sup> I. MacCormack, A. Liu, M. Nozaki, and S. Ryu, Holographic Duals of Inhomogeneous Systems: The Rainbow Chain and the Sine-Square Deformation Model, J. Phys. A: Math. Theor. **52**, 505401 (2019).
- N. Samos Sáenz de Buruaga, S.N. Santalla, J. Rodríguez-Laguna, and G. Sierra, Piercing the rainbow state: Entanglement on an inhomogeneous spin chain with a defect, Phys. Rev. B 101, 205121 (2020).
- N. Samos Sáenz de Buruaga, S.N. Santalla, J. Rodríguez-Laguna, and G. Sierra, Entanglement in non-critical inhomogeneous quantum chains, 2107.12113 [quant-ph] (2021).
- <sup>32</sup> C. Dasgupta and S. K. Ma, Low-temperature properties of the random Heisenberg antiferromagnetic chain, Phys. Rev. B 22, 1305 (1980).
- <sup>33</sup> M. Abramowitz and I. A. Stegun, Handbook of Mathematical Functions: With Formulas, Graphs, Mathematical Tables, Dover Publications (1965).
- <sup>34</sup> M. Ibáñez-Berganza, J. Rodríguez-Laguna, and G. Sierra, Fourier-space entanglement of spin chains, JSTAT 053112 (2016).